Article

Journal of
Nanoscience and Nanotechnology
Vol. 18, 178–187, 2018
www.aspbs.com/jnn

Copyright © 2018 American Scientific Publishers
All rights reserved
Printed in the United States of America

Solar Photocatalytic and Self-Cleaning Performances of $HoVO_4$ Doped ZnO

Kuppulingam Thirumalai[1], Manohar Shanthi[1], and Meenakshisundaram Swaminathan[1, 2, *]

[1] *Photocatalysis Laboratory, Department of Chemistry, Annamalai University, Annamalai Nagar 608002, Tamil Nadu, India*
[2] *Nanomaterials Laborotory, International Research Centre, Kalasalingam University, Krishnankoil 626126, India*

In this article we report preparation of 5 wt% $HoVO_4$ doped ZnO via template-free hydrothermal process and investigated its photocatalytic activity against azo dyes Rhodamine-B (Rh-B), Trypan Blue (TB) and Acid Black 1 (AB 1) in solar light irradiation. The as prepared $HoVO_4$ doped ZnO was characterised by X-ray diffraction (XRD), Field emission scanning electron microscopy (FE-SEM), Field emission Transmission electron microscopy (FE-TEM), Brunauer-Emmett-Teller (BET) surface area measurements, X-ray photoelectron spectroscopy (XPS), Diffused reflectance (DRS) and Photoluminescence (PL) spectroscopy. The SEM images clearly indicate the formation of nanoparticles in the range of 20–50 nm. BET surface area of the $HoVO_4$–ZnO is 2 times that of ZnO. Higher activity of $HoVO_4$–ZnO in natural sunlight may be due to higher visible light absorption of $HoVO_4$–ZnO when compared to undoped ZnO. The results suggested that $HoVO_4$ doping on ZnO has great influence on the photocatalytic activity. The prepared photocatalyst $HoVO_4$–ZnO possesses high stability and reusability without appreciable loss of catalytic activity up to four runs. Significant hydrophobicity of $HoVO_4$–ZnO reveals its self cleaning property.

Scientific Publishers
Delivered by Ingenta

Keywords: Photocatalysis, $HoVO_4$–ZnO, Azo Dyes, Hydrophobicity, Solar Light.

1. INTRODUCTION

Oxidation of organic pollutants in wastewater, particularly azo dyes from the textile industry by utilizing the natural solar energy in photocatalysis has been regarded as a very promising environmentally friendly technique to recover the gradually deteriorating water ecology.[1, 2] Photocatalytic process using novel nanomaterials has been considered as one of the most promising technique to address water pollution and the energy crisis.[3–8] Heterogeneous photocatalytic degradation of industrial organic pollutants from wastewater by semiconductors has attracted extensive attention in the last decade.[9, 10] Among them, semiconductors, TiO_2, ZnO, SnO_2, $BiVO_4$ etc., which drive photocatalysis, have gained a great deal of attention due to their wide application to environmental remediation, mainly for the removal of organic pollutants.[11–14] Suppression of the recombination of photogenerated electron–hole pairs in the semiconductors is essential for improving the efficiency of a photocatalyst. Introducing foreign atoms at a small percentage in the regular crystal lattice of semiconductors or coupling another semiconductor oxide usually produces dramatic changes in their electronic properties by increasing their electron or hole densities.[15–19] Rare earth compounds have received extensive attention because of their potential applications in high-performance luminescent devices, magnets, catalysts, and other functional materials, on the basis of optoelectronic and chemical properties originating from the 4f shell of rare earth ions. Particularly metal orthovanadates of rare earth elements are an important class of inorganic nanomaterials possessing significant interest as complex oxides due to their potential application in diverse fields.[20–23] Holmium doping can effectively improve the photocatalytic activity of TiO_2, as a modified semiconductor photocatalyst.[24–26] Holmium metal doping has been reported to improve the photocatalytic efficiency of ZnO.[27]

Superhydrophobic materials are more suitable for the absorption of organic pollutants from water and catalytic supports in reactions including partial oxidation, isomerization, nitroxidation, esterification, epoxidation, hydrogenation, CO oxidation and as self cleaning materials. The hydrophobicity of the aerogels was studied for their use as self cleaning material.[19, 28]

In continuation of our earlier work on the modification of ZnO[29, 30] for the enhancement of photocatalytic activity

*Author to whom correspondence should be addressed.

 1533-4880/2018/18/178/010 doi:10.1166/jnn.2018.14579

we, herein report a facile hydrothermal-thermal decomposition method to synthesize $HoVO_4$–ZnO nanostructure for photodegradation of three azo dyes such as Rhodamine-B (Rh-B), Trypan Blue (TB) and Acid Black 1 (AB 1). Furthermore its morphological characteristics and hydrophobicity are also discussed.

2. MATERIALS

Zinc nitrate hexahydrate [$Zn(NO_3)_2 \cdot 6H_2O$], Holmium nitrate hexahydrate [$Ho(NO_3)_3 \cdot 6H_2O$], Ammonium metavanadate [NH_4VO_3], Oxalic acid dihydrate [$C_2H_2O_4 \cdot 2H_2O$], Methanol(CH_3OH) (HPLC grade) were obtained from Himedia chemicals. Rhodamine B (Rh-B, molecular formula $C_{28}H_{31}ClN_2O_3$ and molecular weight: 479.01), Trypan Blue (TB, molecular formula $C_{34}H_{28}N_6O_{14}S_4$ and molecular weight: 872.88), Acid Black 1 (AB 1, molecular formula: $C_{22}H_{14}N_6Na_2O_9S_2$; molecular weight: 616.57) from Colour Chem, Pondicherry and ZnO (surface area 5 m^2/g, particle size 4.80 μm) from Merck chemicals were used as received. A gift sample of TiO_2–P25 (80% anatase, 20% rutile with BET surface area 50 $m^2\ g^{-1}$ and mean particle size of 30 nm) was supplied by Evonik, Germany. Deionized distilled water was employed throughout the experiments.

2.1. Preparation of 5 wt% $HoVO_4$–ZnO

0.584 g of NH_4VO_3 (0.05 M) was dissolved in 100 ml of deionized water. Under vigorous agitation, 0.243 g of $Ho(NO_3)_3 \cdot 6H_2O$ solution (0.05 M) was added into the NH_4VO_3 solution at room temperature. The pH of the solution was adjusted to 10 with NaOH for the complete precipitation of $HoVO_4$. The $HoVO_4$ suspension was mixed with 100 mL 0.4 M $Zn(NO_3)_2 \cdot 6H_2O$ (11.90 g) solution and stirred for 30 min. 100 mL of oxalic acid in distilled water (0.6 M) was introduced to the above solution drop wise and stirred for 4 h to ensure complete precipitation of zinc oxalate. The mixed precipitate of zinc oxalate and $HoVO_4$ was treated hydrothermally in a Teflon lined stainless steel autoclave at 115 °C for 12 h with the pressure of 18 psi. Hydrothermally treated precipitate was dried in air at 90 °C for 12 h and calcined at 450 °C for 12 h in a muffle furnace to obtain 5 wt% of $HoVO_4$ in ZnO. Catalysts with 3 wt%, 9 wt% and 12 wt% of $HoVO_4$ were prepared by the addition of appropriate amounts of $Ho(NO_3)_3 \cdot 6H_2O$ and NH_4VO_3 using the above procedure. Among these four catalysts, 5 wt% $HoVO_4$–ZnO was found to be more efficient for the degradation of Rh-B, TB and AB 1 dyes, on primary analysis. Hence this catalyst was characterized using various surface analytical techniques.

2.2. Catalyst Characterization

X-ray diffraction (XRD) patterns were recorded with a Siemens D5005 diffractometer using Cu Kα (k = 0.151 418 nm) radiation. Maximum peak positions were compared with the standard files to identity the crystalline phase. The surface morphology of the $HoVO_4$–ZnO was studied by using a field emission scanning electron microscope (FE-SEM) (Model Carl ZEISS EVO 18). EDS analysis was performed on gold coated samples using a FE-SEM (Model ULTRA-55). FE-TEM images were taken using 200 kV Ultra field emission Transmission Electron Microscope (JEOL-2010). The specific surface areas of the samples were determined through nitrogen adsorption at 77 K on the basis of the BET equation using a Micrometrics ASAP 2020 V3.00 H. X-Ray photoelectron spectra (XPS) of the catalysts were recorded in an ESCA-3 Mark II spectrometer (VG Scientific Ltd., England) using Al Kα (1486.6 eV) radiation as the source. The spectra were referenced to the binding energy of C(1s) (285 eV). A Perkin Elmer LS 55 fluorescence spectrometer was employed to record the photoluminescence (PL) spectra at room temperature. Diffuse reflectance spectra were recorded with Shimadzu UV-2450. UV absorbance measurements were taken using Hitachi-U-2001 spectrometer. The water contact angles were measured using a Drop Shape Analyzer (DSA) (Kruass GmbH, Germany).

2.3. Photocatalytic Experiment

All photocatalytic experiments were carried out under similar conditions on sunny days of April–May 2015 between 11 am and 2 pm. An open borosilicate glass tube of 40 cm height and 20 mm diameter was used as the reaction vessel. 50 mL of dye solution with appropriate amount of $HoVO_4$–ZnO was taken in the reaction vessel and magnetically stirred in the dark for 30 min to attain adsorption–desorption equilibrium between the dye and $HoVO_4$–ZnO. Irradiation was carried out in the open air condition. The suspension was continuously aerated by a pump to provide oxygen and for the complete mixing of reaction solution. During the illumination time no volatility of the solvent was observed. Heat produced in the experiment was dissipated by natural convection using a cooling fan. After dark adsorption the first sample was taken. At specific time intervals, 2 mL of the sample was withdrawn and centrifuged to separate the catalyst. 1 mL of the centrifugate was diluted to 10 mL and its absorbance was measured at 259, 236 and 320 for Rh-B, TB and AB 1 dyes respectively. The absorbance at 259, 236 and 320 nm represent the aromatic content of Rh-B, TB and AB 1 respectively and their decrease indicate the degradation of dye. Solar light intensity was measured for every 30 min and the average light intensity over the duration of each experiment was calculated. The sensor was always set in the position of maximum intensity. The intensity of solar light was measured using LT Lutron LX-10/A Digital Lux meter and the intensity was $1250 \times 100 \pm 100$ lux. The intensity was nearly constant during the experiments. Heber multilamp photoreactor model HML-MP 88 was used for degradation dyes under UV-A light irradiation. The irradiation was carried out using four parallel medium pressure

mercury lamps (4×8 W $= 32$ W) emitting at 365 nm ($I_{UV} = 1.381 \times 10^{-6}$ einstein L^{-1} s^{-1}).

3. RESULTS AND DISCUSSION

3.1. XRD Analysis

XRD can be used as an effective non destructive tool for qualitative and quantitative analysis of the phase structure. Figure 1(a) shows XRD patterns of the prepared ZnO. The 2θ values of ZnO at 31.78, 34.47, 36.27, 47.71, 56.46, 63.20, 66.34, 67.90, 69.03, 72.39, and 76.87° correspond to (100), (002), (101), (101), (110), (103), (220), (112), (201), (004) and (202) planes of Wurtzite ZnO (JCPDS file no. 36–1451).[31] The 2θ values at 25.04, 28.86, 43.44 and 52.65 for the planes (200), (211), (103) and (213) in Figure 1(b) are due to the tetragonal body centered structure of $HoVO_4$ (JCPDS Card No. 82–1973).[32] It should be noted in Figure 1(b) that 2θ angles of (100), (002) and (101) planes for pure ZnO was gradually shifted to the lower diffraction values indicating the appropriate doping of Ho^{3+} ions into the ZnO lattice. This is because of expansion of ZnO lattice caused by the larger radius of Ho^{3+} (1.015 Å) than that of Zn^{2+} (0.704 Å). This structural analysis clearly expose the shifting of lower angle peak position on Ho^{3+} doping, which has a strong evidence of the incorporation of Ho^{3+} into ZnO lattices.[33] The Scherrer formula (Eq. (1)) was used for the calculation of the average crystallite size of $HoVO_4$–ZnO

$$\Phi = \frac{K\lambda}{\beta \cos\theta} \quad (1)$$

Where Φ is the crystallite size, λ is the wavelength of X-ray used; K is the shape factor, β is the full line width at the half-maximum height of the peak, and θ is the Bragg angle. Particles sizes were calculated using all the intense peaks. The average crystallite size of $HoVO_4$–ZnO is found to be 27 nm.

3.2. Structural and Morphological Analysis

The morphology, size and microstructure details of the $HoVO_4$–ZnO were investigated by SEM and TEM techniques. Figure 2 depicts typical information about morphological features of the $HoVO_4$–ZnO through FE-SEM images. Figures 2(a), (b) clearly show that the pure $HoVO_4$–ZnO has large number of uniform spherical shape particles with sizes in the range of 20–50 nm. The incorporation of $HoVO_4$ into the crystal structure of ZnO can reduce the aggregation and crystal size and enhance the shape uniformity of the doped nanoparticles. The SEM images of $HoVO_4$–ZnO further confirm the presence of many of the cavities in its lattice structure (Fig. 2(a)). These different morphological structures of $HoVO_4$–ZnO help to increase the photocatalytic activity.

IP: 128.122.151.55.44 On: Sun, 05 A
Copyright: American Scienti
Delivered by Inge

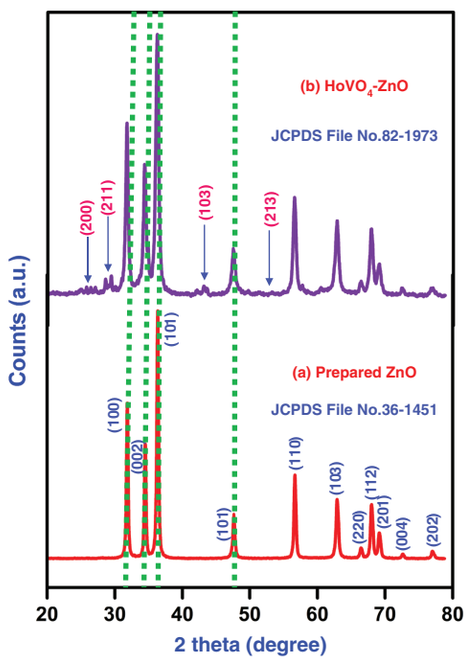

Figure 1. XRD patterns of (a) Prepared ZnO and (b) 5 wt% $HoVO_4$–ZnO.

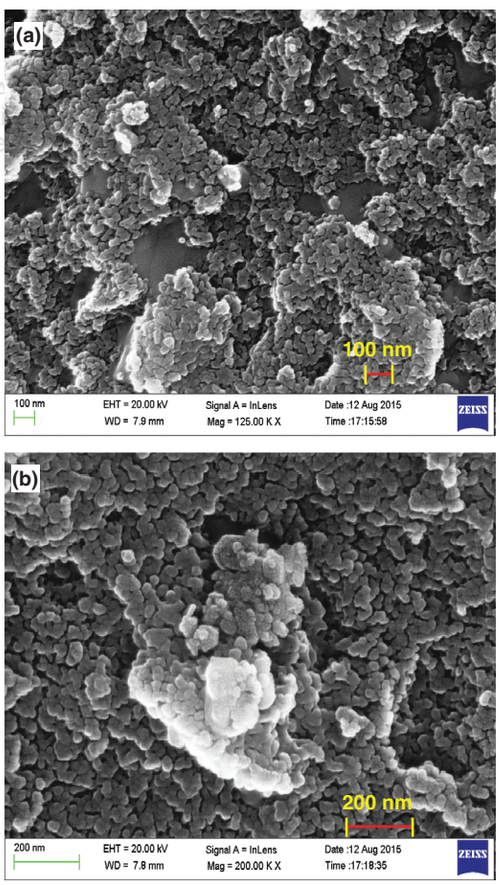

Figure 2. FE-SEM images of $HoVO_4$–ZnO at different magnifications (a) 100 nm and (b) 200 nm.

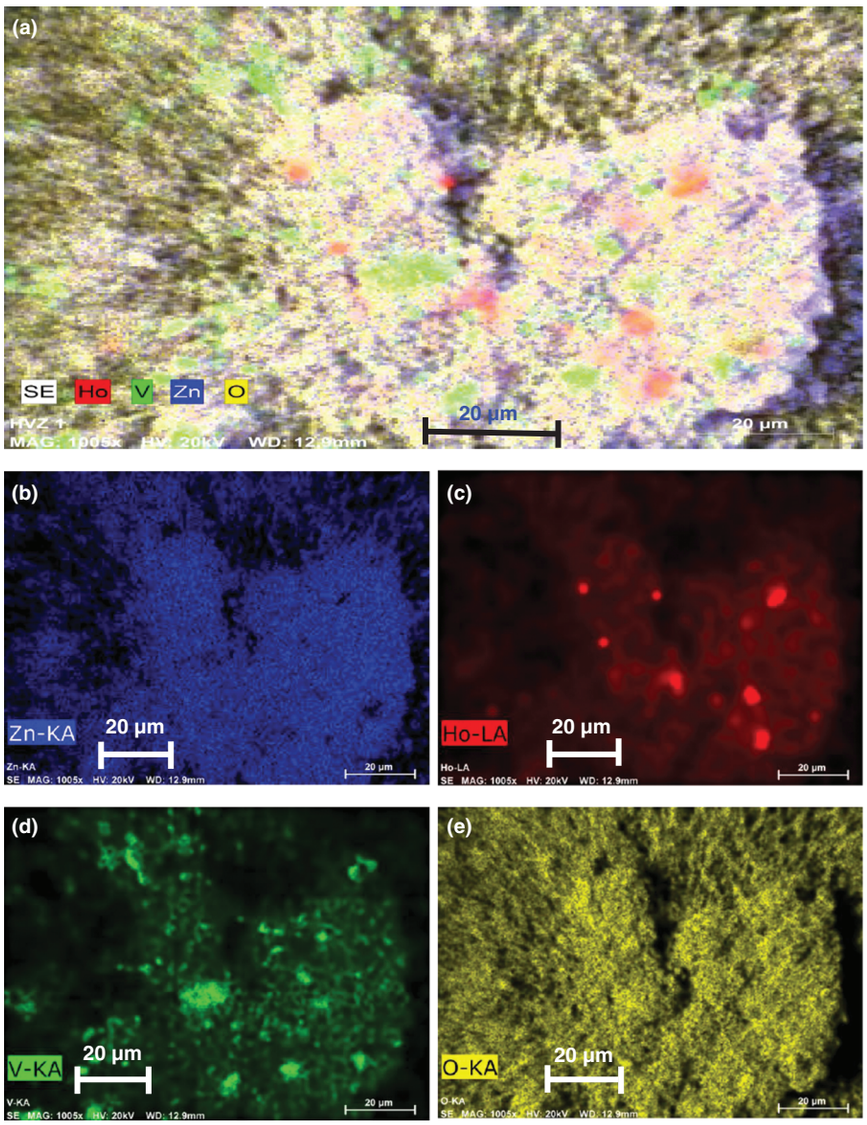

Figure 3. Elemental colour mapping images of $HoVO_4$–ZnO (a) $HoVO_4$–ZnO composite, (b) Zn, (c) Ho, (d) V and (e) O.

Figure 3(a) clearly depicts the distribution of Ho, Zn, V and O in the surface of the catalyst by FE-SEM elemental colour mapping. Figures 3(b)–(e) show individual elemental colour mapping of Zn, Ho, V and O. It implies from Figures 3(b) and (e) that Zn and O are present in higher density and there is a homogenous distribution of elements. This analysis also shows the purity of the prepared $HoVO_4$–ZnO nanomaterial. The energy dispersive spectroscopy (EDS) results confirm the presence of Ho, Zn, V and O in $HoVO_4$–ZnO.

Furthermore the internal morphology and microstructure of as prepared $HoVO_4$–ZnO were revealed by FE-TEM images, shown in Figure 4. The low-magnification TEM image (0.2 μm) reveals the presence of $HoVO_4$ (dark shade) on the ZnO lattice (gray) (Fig. 4(a)). Figure 4(b) also confirms that the particles are present in the range of 20–50 nm. As can be seen from Figure 4(c) prepared catalyst has particles with hexagonal structure. From the Figure 4(d), tube-like particles are seen at a particular location.

AFM images of $HoVO_4$–ZnO with 5 μm $\times$ 5 μm regions, shown in Figure 5, clearly indicate the surface roughness and porosity of the catalyst. The average surface roughness was found as 31.20 nm. The existence of nano-sized particles in the $HoVO_4$–ZnO nanomaterial is more clearly reflected in its 2D AFM image (Fig. 5(a)). The surface roughness of the prepared $HoVO_4$–ZnO is shown in 3D AFM image (Fig. 5(b)). Higher surface roughness and lower particle size reveals that the surface is highly porous in nature. The surface porosity and roughness in the photocatalyst permits the adsorption of dye molecules onto the surface, thereby increasing the photodegradation rate.

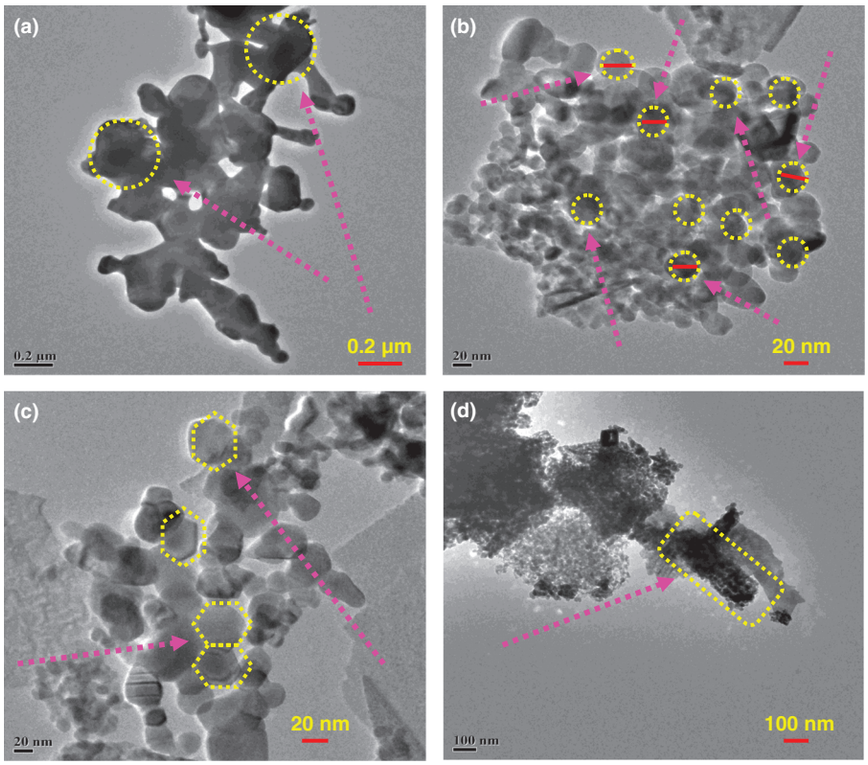

Figure 4. FETEM images of $HoVO_4$–ZnO (a) 0.2 μm (b, c) 20 nm and (d) 100 nm.

IP: 191.101.55.44 On: Sun, 05 Aug 2018 00:26:28
Copyright: American Scientific Publishers
Delivered by Ingenta

The pore structure of the $HoVO_4$–ZnO photocatalyst was investigated by nitrogen adsorption–desorption isotherms and the pore size distribution was calculated by Barrett-Joyner-Halenda (BJH) method. The N_2 adsorption/desorption isotherms of the synthesized $HoVO_4$–ZnO (Fig. 6(a)) exhibit a type III isotherm with a H3 hysteresis loop according to the classification of IUPAC. A sharp increase in the adsorption volume of N_2 was observed and located in the P/P_0 range of 0.80–0.99, which can be attributed to the capillary condensation, indicating the good homogeneity of the sample and macro pore size since the P/P_0 position of the inflection point is related to the pore size. The average pore radius of $HoVO_4$–ZnO is found to be 215 Å (Fig. 6(b)). The pore size distribution of the $HoVO_4$–ZnO catalyst thus shows the macroporous structure. Surface area measurements, made by the BET method, provide the specific surface area of $HoVO_4$–ZnO as 20.5 m^2g^{-1}, which is 2 times that of prepared ZnO (10.2 m^2g^{-1}). It is to be emphasized that this type of isotherm indicates the presence of macroporous structure in $HoVO_4$–ZnO. This porous structure with high surface area (20.5 m^2g^{-1}) leads to higher photocatalytic activity.[34]

3.3. X-ray Photoelectron Spectral Analysis

The elements present and their valence states can be found with the help of X-ray photoelectron spectroscopy. Figure 7(a) shows the survey spectrum of $HoVO_4$–ZnO photocatalyst and it proves that prepared nanomaterial mainly consists of Holmium (Ho), Zinc (Zn), Oxygen (O) and Vanadium (V). Peaks of other elements are not observed. Figure 7(b) shows Zn $2p$ signal at 1045.6 and 1022.5 eV corresponding to Zn $2p_{1/2}$ and Zn $2p_{3/2}$ orbitals.[35] In Figure 7(c), the peak centred at 159.7 eV is ascribed to Ho $4d$ and is in good agreement with the Ho $4d_{5/2}$.[36] Therefore, this peak is related to the Ho^{3+} ions in the ZnO lattice, which confirms the proper incorporation of Ho^{3+} into the ZnO lattice. Binding energy peak of O $1s$ (Fig. 7(d)) is asymmetric and can be fitted to two symmetrical peaks (locating at 531.1 and 532.7 eV), for two different kinds of O species in the sample. These two peaks should be associated with the lattice oxygen (OL) of Ho–O–Zn and chemisorbed oxygen (OH) caused by the surface hydroxyl groups which is helpful to improve the photocatalytic activity of $HoVO_4$–ZnO.[37] The V $2p_{1/2}$ and V $2p_{3/2}$ peaks (Fig. 7(e)) centred at 525.6 and 518.1 eV are assigned to V^{4+} of $HoVO_4$ and it is confirmed with the reported values.[38]

3.4. Optical Properties of $HoVO_4$–ZnO

To find out the optical properties, UV-vis diffuse reflectance and photoluminescence spectra for the ZnO and $HoVO_4$–ZnO catalysts were recorded. Figure 8(a) shows the diffuse reflectance spectrum of $HoVO_4$–ZnO. Any impurity in the semiconductor oxide can form intermittent band energy levels and this leads to the decrease of bandgap energy, which increases the UV-visible

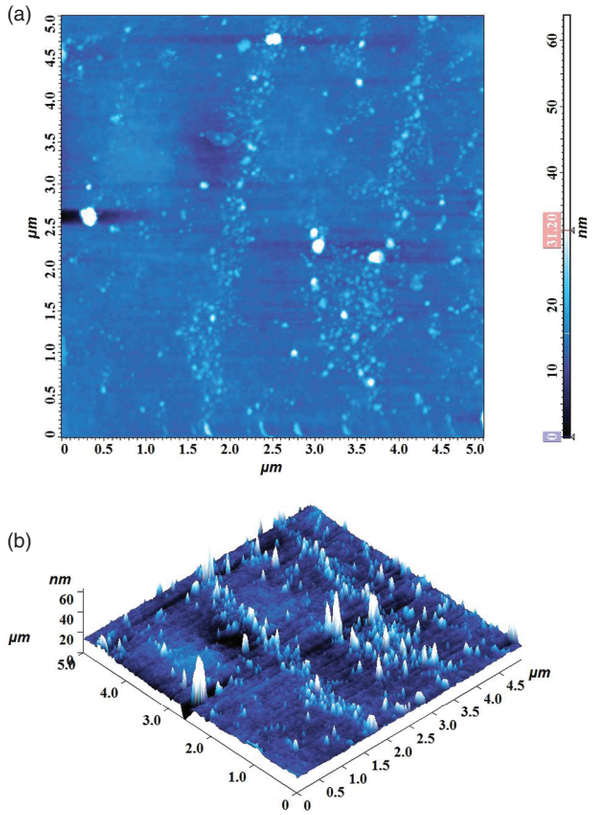

Figure 5. AFM images of the surface morphology of 5 $\mu m \times 5$ μm region of the $HoVO_4$–ZnO. (a) 2D image and (b) 3D image of $HoVO_4$–ZnO.

IP: 191.101.55.44 On: Sun, 19 Aug 2018 ... Delivered by Ingenta

absorption. As seen in Figure 8(a), prepared nanomaterial $HoVO_4$–ZnO (Fig. 8a(i)) shows reduced reflectance spectrum (increased absorption) both in UV and visible region compared to prepared ZnO (Fig. 8a(ii)). Hence the band gap energy is less than prepared ZnO. This reveals that prepared $HoVO_4$–ZnO catalyst can be used as UV and visible active material. UV-Vis spectra in the diffuse reflectance mode (R) were transformed to the Kubelka-Munk function $F(R)$ to separate the extent of light absorption from scattering. The band gap energy (2.82 eV) was obtained from the plot of the modified Kubelka-Munk function $(F(R)E)^{1/2}$ versus the energy of the absorbed light E (Eq. (2)) (Fig. 8(b))

$$F(R)E^{1/2} = \left[\frac{(1-R)^2}{2R} \times h\nu\right]^{1/2} \quad (2)$$

Photocatalysts generate electrons and holes on irradiation by light, and the recombination of electrons and holes release energy in the form of fluorescence emission. There is a strong correlation between PL intensity and photocatalytic activity as reported earlier.[39] Lower fluorescence emission intensity implies lower electron–hole recombination rate. The emission spectrum of prepared ZnO and $HoVO_4$–ZnO are shown in Figures 9(a) and (b) respectively. Both prepared ZnO and $HoVO_4$–ZnO exhibit predominantly blue emission with peaks centered at 418, 446 and 530 nm. In particularly, PL emission peak at 418, 446 and 530 nm are assigned to the $^5I_8 \rightarrow {}^5G_5$; $^5I_8 \rightarrow {}^5G_6$, $^3K_8$; and $^5I_8 \rightarrow {}^5S_2$, $^5F_4$ transitions, respectively. These PL peaks result from sharp f–f absorption lines typical for holmium ions.[40] It can be seen that the positions of the peaks are similar, while PL intensities are different. The PL intensity of prepared ZnO at 418 nm due to electron–hole recombination is higher than that of $HoVO_4$–ZnO. The decreased emission intensity in $HoVO_4$–ZnO, implies that the recombination of charge carriers is suppressed by doped $HoVO_4$ on ZnO, which leads to the enhanced photoactivity.

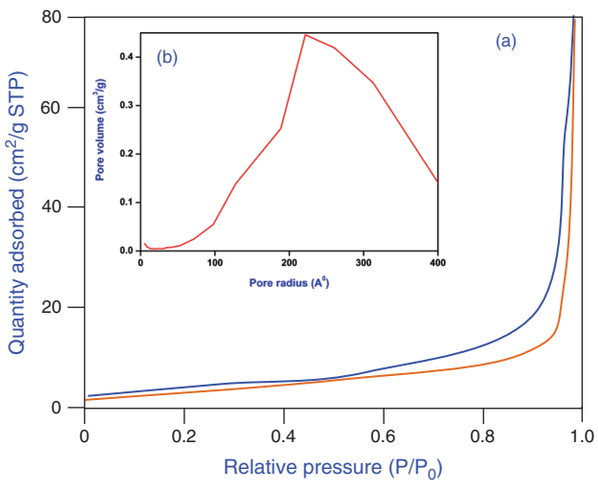

Figure 6. (a) N_2 adsorption–desorption isotherm of $HoVO_4$–ZnO and (b) Pore volume/Pore radius of $HoVO_4$–ZnO.

3.5. Photodegradation Studies

Photocatalytic degradation of Rh-B under different conditions with increasing irradiation times is displayed in Figure 10. Dye is resistant to self photolysis and for the same experiment with $HoVO_4$–ZnO in the dark, a decrease (12%) in dye concentration was observed. This is because of the adsorption of dye on the catalyst. Rh-B undergoes 96% degradation in the presence of $HoVO_4$–ZnO under natural sunlight in 75 min. But, prepared ZnO, TiO_2–P25, and undoped $HoVO_4$ shows 64%, 62% and 54% degradations, respectively in 75 min. This results shows prepared 5 wt% $HoVO_4$–ZnO nanomaterial is most efficient for degradation of Rh-B dye relative to other photocatalysts (Fig. 10). We also compared the efficiency of prepared catalyst 5 wt% $HoVO_4$–ZnO with solar and UV irradiation, it is found that $HoVO_4$–ZnO shows higher activity in solar irradiation (96%) than in UV light of 365 nm (86%). To test the activity of the catalyst on the degradations of other azo dyes, we had carried out the experiments on the degradation of TB and AB 1 under the same conditions. Degradations of Rh-B, TB and AB 1 using $HoVO_4$–ZnO at different irradiation times were compared. Rh-B, TB and AB 1 undergo 96%, 95% and 97% degradations

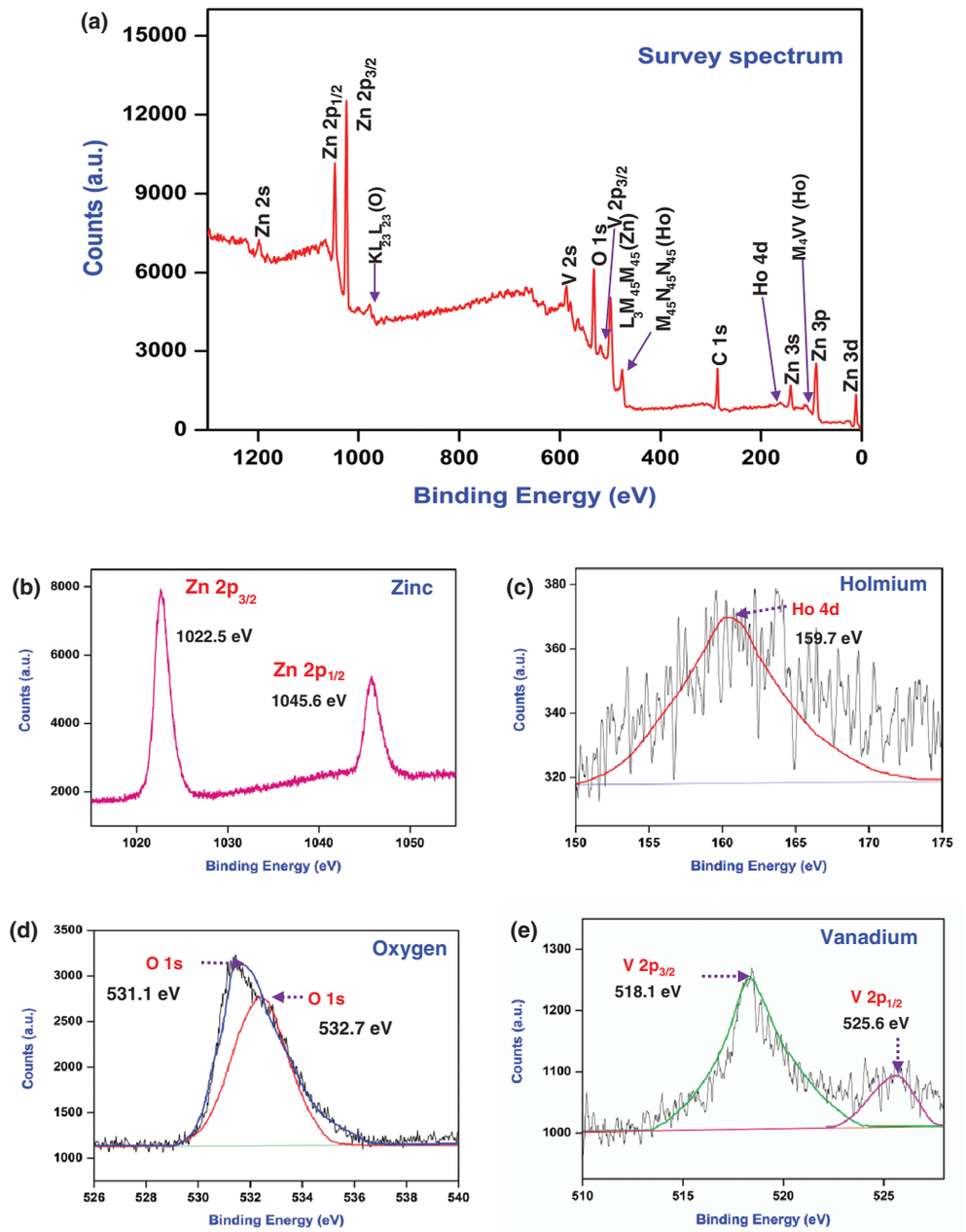

Figure 7. XPS analysis of $HoVO_4$–ZnO (a) Survey spectrum (b) Zn 2*p* (c) Ho 4*d* (d) O 1*s* and (e) V 2*p*.

respectively in 75 min. The results reveal that this catalyst is efficient in the degradation of azo dyes.

The solution pH plays a crucial role in the photocatalytic degradation. The effect of pH on the photodegradation of Rh-B was studied in the pH range 3–11 and the results reveal 44, 62, 96, 77 and 60% degradations at pH 3, 5, 7, 9 and 11 respectively. The degradation efficiency is high at pH 7 and it decreases when the pH is above or below 7. Low removal efficiency at acidic pH range may be due to the dissolution of ZnO in $HoVO_4$–ZnO. It shows prepared catalyst is more advantageous than undoped ZnO in the degradation of Rh-B because it has maximum efficiency at the neutral pH 7.

The reusability of $HoVO_4$–ZnO was tested for the degradation of Rh-B, TB and AB 1 dyes under the same reaction environment. After complete degradation, the catalyst was separated and washed with deionized water. The recovered catalyst was dried in hot air oven at 100 °C for 3 h and used for a second run. Figure 11 shows the results of Rh-B, TB and AB 1 degradation for four successive runs.

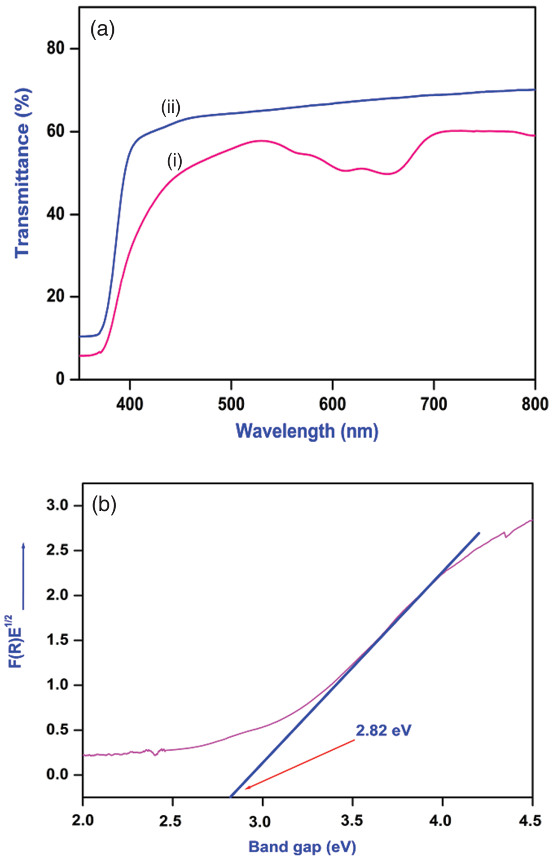

Figure 8. (a) Diffused reflectance spectrum of $HoVO_4$–ZnO and (b) K-M bandgap plot of $HoVO_4$–ZnO.

IP: 191.101.55.44 On: Sun
Copyright: American S
Delivered by Ingenta

Dye degradation percentages of Rh-B are 96, 95, 94 and 94 in 75 min for the first, second, third and fourth run respectively. In TB dye degradation $HoVO_4$–ZnO shows 95, 94, 93 and 93% degradations in 75 min for the first four cycles. $HoVO_4$–ZnO gives 97, 96, 95 and 95% degradations in AB 1 dye for first, second, third and fourth run respectively in 75 minutes. There is no significant change in the degradation efficiency of $HoVO_4$–ZnO after second run for all the three azo dyes.

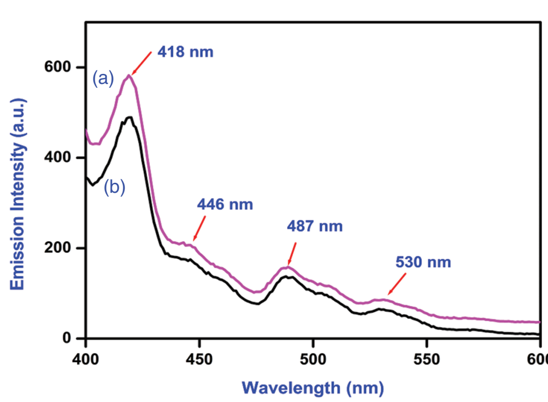

Figure 9. Photoluminescence spectrum of $HoVO_4$–ZnO (a) prepared ZnO and (b) $HoVO_4$–ZnO.

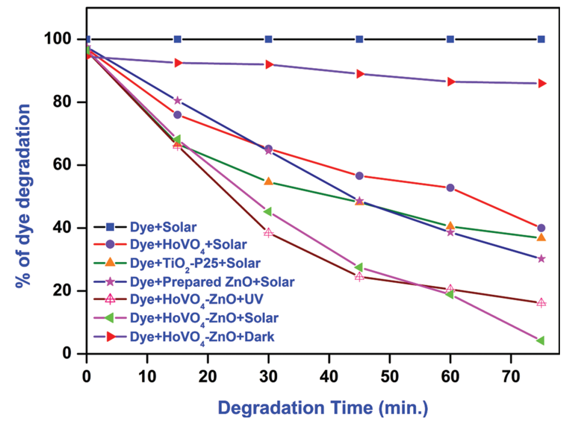

Figure 10. Primary analysis: Rh-B dye concentration $= 3 \times 10^{-4}$ M, catalyst suspended $= 3$ g L^{-1}, pH $= 7$, airflow rate $= 8.1$ mL s^{-1} and irradiation time 75 min, $I_{solar} = 1250 \times 100$ Lux ± 100, $I_{UV} = 1.381 \times 10^{-6}$ einstein L^{-1} s^{-1}.

3.5.1. Mechanism of Photodegradation

The presence of f electrons is acknowledged as essential for an optimal photocatalytic performance. This is because rare earth metal ions with incompletely occupied $4f$ and empty $5d$ orbitals often serve as a catalyst or promotes catalysis.[41] Furthermore, better photocatalytic activity in orthovanadates is observed to be due to the presence of regular VO_4 tetrahedra, which is beneficial for the charge transfer to surface of material.[42] DRS spectrum of $HoVO_4$ shows increased absorption profile compared to undoped ZnO. The absorption edge shifts to a longer wavelength depending on the content of $HoVO_4$. The improved photocatalytic activity for the $HoVO_4$–ZnO is attributed to efficient electron trapping followed by electron transfer. The dopant ion (Ho^{3+}) is reduced (Ho^{2+}) upon trapping an electron, which is then followed by the transfer of the electron to O_2 to form a radical species ($O_2^{\bullet-}$) with

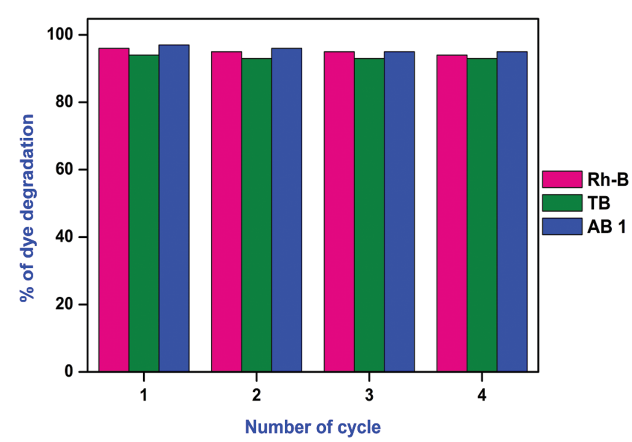

Figure 11. Reusability of $HoVO_4$–ZnO on degradation of dyes Rh-B, TB and AB 1: dye concentration: Rh-B $= 3 \times 10^{-4}$ M, TB $= 1 \times 10^{-4}$ M and AB 1 $= 1 \times 10^{-4}$ M catalyst suspended $= 3$ g L^{-1}, pH $= 7$, airflow rate $= 8.1$ mL s^{-1} and irradiation time 75 min, $I_{solar} = 1250 \times 100$ Lux ± 100.

simultaneous reoxidation of the dopant ion. The radical is able to efficiently undergo other photocatalytic processes leading to the degradation of the organic species. The results may be attributed to the charge transfer between $4f$ electrons of Ho ion and the conduction (or valence) band of undoped material.[43] As self-sensitive dyes, the excited Rh-B* molecules after irradiation, chemisorbed on the surface of photocatalysts may inject electrons into the conduction band of ZnO, which enhance the visible photoactivity of catalyst.[44] The decreased emission intensity in $HoVO_4$–ZnO, also confirm the suppression of recombination of electron–hole by $HoVO_4$ particles, and this leads to enhanced phtocatalytic activity. AFM studies also prove that the surface of the synthesized photocatalyst is very rough and porous in nature and this may assist the trapping of the electrons generated during photo process and subsequently generate radicals to degrade the organic molecules on the surface of the catalyst.

3.6. Contact Angle Measurements

Surface non-wettability or the hydrophobicity of the catalyst is exposed by water contact angle. If a surface has a contact angle with water greater than 90°, then the surface is classed as hydrophobic and if the contact angle is less than 90°, the surface is hydrophilic. Water contact angles were determined using glass slides coated with TEOS, TEOS + ZnO and TEOS + $HoVO_4$–ZnO to determine the hydrophobicity of the catalysts. Figure 12 shows the images of water drops on coated and uncoated glass slides. Water contact angle (WCA) of 21.5° on uncoated glass slide shows the hydrophilicity and this WCA increases gradually on glass slides coated with TEOS (50.2°), TEOS + ZnO (73.4°) and TEOS + $HoVO_4$–ZnO (109.5°). Surface coated with TEOS + $HoVO_4$–ZnO has more hydrophobic character. In TEOS, the O–Si–O groups are modified by $HoVO_4$–ZnO to make the surface rougher, stable and non-wettable. Hence the contact angle increases above 90° exhibiting the hydrophobicity of the catalyst. This surface non-wettability leads to a self cleaning property of the catalyst.

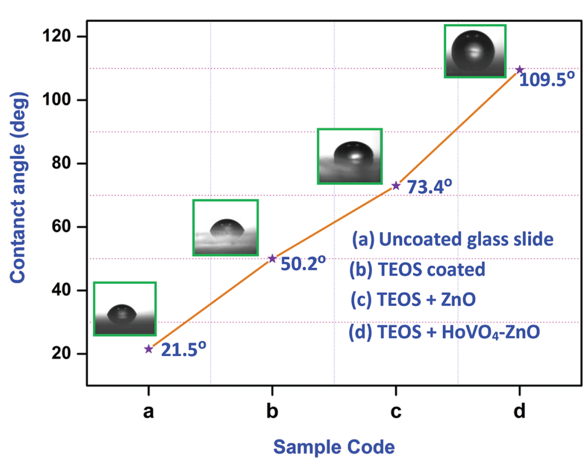

Figure 12. Water contact angle measurements (a) uncoated glass slide, (b) TEOS coated glass slide, (c) TEOS + ZnO coated glass slide and (d) TEOS + $HoVO_4$–ZnO coated glass slide.

4. CONCLUSIONS

In summary, a new solar light active $HoVO_4$–ZnO photocatalyst was synthesized by a simple hydrothermal-thermal decomposition method and characterized by the various analytical techniques. The XRD pattern confirmes ZnO having hexagonal wurtzite structure and $HoVO_4$ tetragonal body-centered structure with average crystallite size of 27 nm. FESEM and FETEM images further prove the morphology of prepared $HoVO_4$ doped ZnO as hexagonal and sphere shaped particles in regular arrangement. Elemental colour mapping studies reveals the presence and homogeneous distribution of Ho, Zn, V and O in $HoVO_4$–ZnO. AFM images reveal the higher surface roughness of $HoVO_4$–ZnO, leading to large surface area. BET surface area of the $HoVO_4$–ZnO is 2 times higher than that of prepared ZnO. During photocatalysis, Ho^{3+} ions acted as electron scavengers and suppressed electron–hole recombination, which enhanced the activity of $HoVO_4$–ZnO in the degradation of azo dyes Rh-B, TB and AB 1. $HoVO_4$–ZnO was found to be a stable and reusable catalyst. $HoVO_4$–ZnO forms WCA of 109.5° showing its self cleaning property. $HoVO_4$–ZnO will be very useful for industries for effective treatment of effluents containing dyes and organic pollutants and also as a self-cleaning material.

IP: 191.101.55.44 On: Sun, 05 Aug 2018 00:26:28
Copyright: American Scientific Publishers
Delivered by Ingenta

Acknowledgment: Authors are thankful to the CSIR, New Delhi, for the financial support through research Grant no. 02 (0144)/13/EMR-II. Authors are grateful to International Research Centre, Kalasalingam University, Krishnankoil, Tamil Nadu for availing FE-SEM facility.

References and Notes

1. T. Kamegawa, H. Imai, and H. Yamashita, *Bull. Chem. Soc. Jpn* 89, 743 (**2016**).
2. M. Muruganandham, P. S. Suri, M. Sillanpaa, J. J. Wu, B. Ahmmad, S. Balachandran, and M. Swaminathan, *J. Nanosci. Nanotech.* 14, 1898 (**2014**).
3. W. Fan, Q. Zhang, and Y. Wang, *Phys. Chem. Chem. Phys.* 15, 2632 (**2013**).
4. H. Kisch, *Angew. Chem. Int. Ed.* 52, 812 (**2013**).
5. K. Maeda and K. Domen, *Bull. Chem. Soc. Jpn* 89, 627 (**2016**).
6. Y. Hong, Y. Jiang, C. Li, W. Fan, X. Yan, M. Yan, and W. Shi, *Appl. Catal. B Environ.* 180, 663 (**2016**).
7. S. Song, B. Cheng, N. Wu, A. Meng, S. Cao, and J. Yu, *Appl. Catal. B Environ.* 181, 71 (**2016**).
8. T. Takayama, A. Iwase, and A. Kudo, *Bull. Chem. Soc. Jpn* 88, 538 (**2015**).
9. Y. Wang, Z. Wang, S. Muhammad, and J. He, *CrystEngComm.* 14, 5065 (**2012**).
10. B. Subash, B. Krishnakumar, B. Sreedhar, M. Swaminathan, and M. Shanthi, *Superlattices Microstruct.* 54, 155 (**2012**).
11. D. Sarkar, C. K. Ghosh, S. Mukherjee, and K. K. Chattopadhyay, *ACS Appl. Mater. Interfaces* 5, 331 (**2013**).

12. E. T. Deva Kumar, K. Thirumalai, R. Aravindhan, M. Swaminathan, J. Raghava Rao, and B. U. Nair, *RSC Adv.* 5, 60926 **(2015)**.
13. S. P. Kim, M. Y. Choi, and H. C. Choi, *Appl. Surf. Sci.* 357, 302 **(2015)**.
14. S. Liu, K. Yin, W. Ren, B. Cheng, and J. Yu, *J. Mater. Chem.* 22, 17759 **(2012)**.
15. X. Pian, B. Lin, Y. L. Chen, J. D. Kuang, K. Z. Zhang, and L. M. Fu, *J. Phys. Chem. C* 115, 6531 **(2011)**.
16. S. Balachandran and M. Swaminathan, *J. Phys. Chem. C* 116, 26306 **(2012)**.
17. R. Georgekutty, M. K. Seery, and S. C. Pillai, *J. Phys. Chem. C* 112, 13563 **(2008)**.
18. A. Senthilraja, B. Subash, P. Dhatshanamurthi, M. Swaminathan, and M. Shanthi, *Spectrochim. Acta, Part A* 138, 3 **(2015)**.
19. S. Balachandran, K. Thirumalai, and M. Swaminathan, *RSC Adv.* 4, 27642 **(2014)**.
20. Z. Xu, C. Li, Z. Hou, C. Peng, and J. Lin, *CrystEngComm.* 13, 474 **(2011)**.
21. D. Errandonea, S. N. Achary, J. P. Porres, and A. K. Tyagi, *Inorg Chem.* 52, 5464 **(2013)**.
22. Z. Xu, B. Feng, Y. Gao, Q. Zhao, D. Sun, X. Gao, K. Li, F. Ding, and Y. Sun, *CrystEngComm.* 14, 5530 **(2012)**.
23. A. W. Xu, Y. P. Fang, L. P. You, and H. Q. Liu, *J. Am. Chem. Soc.* 125, 1494 **(2003)**.
24. W. Zhou and Y. He, *Chem. Eng. J.* 179, 412 **(2012)**.
25. H. Cai, G. Liu, W. Lu, X. Li, L. Yu, and D. Li, *J. Rare Earth* 26, 71 **(2008)**.
26. X. Liu, P. Fang, Y. Liu, Z. Liu, D. Lu, Y. Gao, F. Chen, D. Wang, and Y. Dai, *J. Mater. Sci.* 49, 8063 **(2014)**.
27. A. Khataee, S. Saadi, B. Vahid, and S. W. Joo, *J. Ind. Eng. Chem.* 35, 167 **(2016)**.
28. J. Zhu, J. Xie, X. Lu, and D. Jiang, *Colloids Surf. A* 342, 97 **(2009)**.
29. K. Thirumalai, S. Balachandran, and M. Swaminathan, *Mater. Chem. Phys.* 183, 191 **(2016)**.
30. K. Thirumalai, E. T. Deva Kumar, R. Aravindhan, J. Raghava Rao, and M. Swaminathan, *Surf. Interface* 5, 30 **(2016)**.
31. S. Yang, D. L. Han, M. Gao, J. H. Yang, and Bayanheshig, *CrystEngComm.* 16, 6896 **(2014)**.
32. B. C. Chakoumakos, M. M. Abraham, and L. A. Boatner, *J. Solid-state. Chem.* 109, 197 **(1994)**.
33. S. Y. Bae, H. W. Seo, and J. Park, *J. Phys. Chem. B* 108, 5206 **(2004)**.
34. Y. Miao, H. Zhang, S. Yuan, Z. Jiao, and X. Zhu, *J. Colloid Interface Sci.* 462, 9 **(2016)**.
35. M. Chen, X. Wang, Y. H. Yu, Z. L. Pei, X. D. Bai, C. Sun, R. F. Huang, and L. S. Wen, *Appl. Surf. Sci.* 158, 134 **(2000)**.
36. W. Zhou and Y. He, *Chem. Eng. J.* 179, 412 **(2012)**.
37. J. Shi, J. Zheng, Y. Hu, and Y. Zhao, *Kinet. Catal* 49, 279 **(2011)**.
38. M. C. Biesinger, L. W. M. Lau, A. R. Gerson, and R. St. C. Smart, *Appl. Surf. Sci.* 257, 887 **(2010)**.
39. C. Ren, B. Yang, M. Wu, J. Xu, Z. Fu, Y. Lv, T. Guo, Y. Zhao, and C. Zhu, *J. Hazard. Mater.* 182, 123 **(2010)**.
40. G. Leniec, S. M. Kaczmarek, M. Berkowski, M. Głowacki, T. Skibinski, A. Suchocki, and Y. A. Zhydachevskii, *J. Cryst. Growth* 401, 177 **(2014)**.
41. M. Oshikiri, J. Ye, and M. Boero, *J. Phys. Chem. C* 118, 8331 **(2014)**.
42. S. Mahapatra, G. Madras, and T. N. Guru Row, *J. Phys. Chem C* 111, 6505 **(2007)**.
43. Z. Shi, Y. Xiang, X. Zhang, and S. Yao, *Photochem. Photobiol.* 87, 626 **(2011)**.
44. S. M. Lam, J. C. Sin, A. Z. Abdullah, and A. R. Mohamed, *Desalin. Water. Treat.* 41, 131 **(2012)**.

IP: 191.101.55.44 On: Sun, 05 Aug 2018 00:26:28
Copyright: American Scientific Publishers
Delivered by Ingenta

Received: 25 November 2016. Accepted: 23 December 2016.